Inorganic Chemistry

Article

pubs.acs.org/IC

Unprecedented Trapping of Difluorooctamolybdate Anions within an α-Polonium Type Coordination Network

Olena V. Sharga,[†] Andrey B. Lysenko,*[,†] Marcel Handke,[‡] Harald Krautscheid,[‡] Eduard B. Rusanov,[§] Alexander N. Chernega,[§] Karl W. Krämer,[⊥] Shi-Xia Liu,*[,⊥] Silvio Decurtins,[⊥] Adam Bridgeman,[∥] and Konstantin V. Domasevitch[†]

[†]Inorganic Chemistry Department, Taras Shevchenko National University of Kyiv, Volodimirska Str. 64, Kyiv 01033, Ukraine

[‡]Institut für Anorganische Chemie, Universität Leipzig, Johannisallee 29, D-04103 Leipzig, Germany

[§]Institute of Organic Chemistry, Murmanska Str. 5, Kyiv 02660, Ukraine

[⊥]Departement für Chemie und Biochemie, Universität Bern, Freiestrasse 3, CH-3012 Bern, Switzerland

[∥]School of Chemistry, The University of Sydney, Sydney, New South Wales 2006, Australia

Supporting Information

ABSTRACT: New fluorinated hybrid solids $[Mo_2F_2O_5(tr_2pr)]$ (**1**), $[Co_3(tr_2pr)_2(MoO_4)_2F_2]\cdot 7H_2O$ (**2**), and $[Co_3(H_2O)_2(tr_2pr)_3(Mo_8O_{26}F_2)]\cdot 3H_2O$ (**3**) (tr_2pr = 1,3-bis(1,2,4-triazol-4-yl)propane) were prepared from the reaction systems consisting of $Co(OAc)_2/CoF_2$ and $MoO_3/(NH_4)_6Mo_7O_{24}$, as Co^{II} and Mo^{VI} sources, in water (**2**) or in aqueous HF (**1**, **3**) employing mild hydrothermal conditions. The tr_2pr ligand serves as a conformationally flexible tetradentate donor. In complex **1**, the octahedrally coordinated Mo atoms are linked in the discrete corner-sharing $\{Mo_2(\mu_2\text{-}O)F_2O_4N_4\}$ unit in which a pair of tr-heterocycles (tr = 1,2,4-triazole) is arranged in cis-positions opposite to "molybdenyl" oxygen atoms. The *anti*−*anti* conformation type of tr_2pr facilitates the tight zigzag chain packing motif. The crystal structure of the mixed-anion complex salt **2** consists of trinuclear $[Co_3(\mu_3\text{-}MoO_4)_2(\mu_2\text{-}F)_2]$ units self-assembling in Co^{II}-undulating chains (Co···Co 3.0709(15) and 3.3596(7) Å), which are cross-linked by tr_2pr in layers. In **3**, containing condensed oxyfluoromolybdate species, linear centrosymmetric $[Co_3(\mu_2\text{-}tr)_6]^{6+}$ SBUs are organized at distances of 10.72−12.45 Å in an α-Po-like network using bitopic tr-linkers. The octahedral $\{N_6\}$ and $\{N_3O_3\}$ environments of the central and peripheral cobalt atoms, respectively, are filled by triazole N atoms, water molecules, and coordinating $[Mo_8O_{26}F_2]^{6-}$ anions. Acting as a tetradentate O-donor, each difluorooctamolybdate anion anchors four $[Co_3(\mu_2\text{-}tr)_6]^{6+}$ units through their peripheral Co-sites, which consequently leads to a novel type of a two-nodal 4,10-c net with the Schläfli symbol $\{3^2.4^3.5\}\{3^4.4^{20}.5^{16}.6^5\}$. The 2D and 3D coordination networks of **2** and **3**, respectively, are characterized by significant overall antiferromagnetic exchange interactions (J/k) between the Co^{II} spin centers on the order of −8 and −4 K. The $[Mo_8O_{26}F_2]^{6-}$ anion is investigated in detail by quantum chemical calculations.

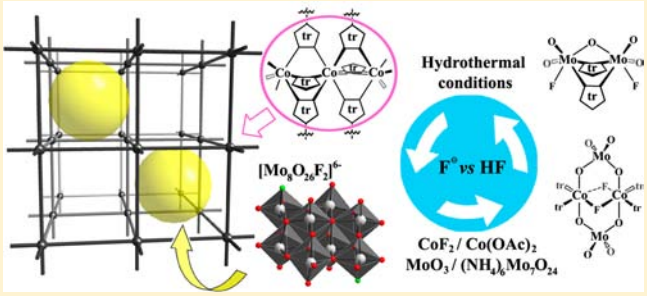

INTRODUCTION

Molybdenum oxide fluoride polyanions are attractive building blocks that represent an intriguing challenge in the engineering of new types of solids to be explored in materials chemistry, for example, in areas of nonlinear optics and ferroelectrics.[1] In this context, the ability to introduce the molybdenum oxide fluoride species into metal−organic frameworks (MOFs) for the development of a wide scope of novel organic−inorganic hybrid solids is of particular interest. Most of the previous efforts were focused on the chemistry of noncentrosymmetric organic−inorganic compounds containing the distorted *cis*-$[MoO_2F_4]^{2-}$ octahedral anion and its analogues.[2] Only some particular examples dealt with the structural behavior of di- and tetranuclear anions, $[Mo_2O_6F_3]^{2-3}$ and $[Mo_4O_{12}F_2]^{2-}$,[4] in copper(II)−pyridine and copper(II)−terpyridine types of complexes, whereas polynuclear oxide fluoride species, such as $[Mo_6O_{18}F_6]^{6-}$, $[Mo_7O_{22}F_3]^{5-}$,[5] $[Mo_8O_{26}F_2]^{6-}$,[6] or $[Mo_{16}O_{53}F_2]^{12-}$,[7] are so far only known as simple alkali-metal or alkyl-ammonium salts. Definitely, this situation is in high contrast to that of classical isopolymolybdate clusters, many of which form a tremendous diversity of extended coordination solids.[8] The synthesis of MOFs incorporating the polynuclear molybdenum oxide fluoride species is a complex process that usually proceeds under hydrothermal conditions and still remains to be very challenging. In essence, it requires a precise and specific interplay between multiple reaction components and parameters, such as the choice of fluoride and molybdenum sources, the concentration of reactants and their ratio, the pH value of the reaction media, etc. Special attention has to be paid

Received: April 17, 2013
Published: July 12, 2013

Table 1. Synthetic Conditions for the Preparation of Compounds 2 and 3[a]

	Co(II) precursor	Mo(VI) precursor	additional F^- source	molar ratio $Co^{II}/Mo^{VI}/F^-/tr_2pr$	products (ratio, crystal shape)
1	$CoF_2·4H_2O$, 0.80 mmol	$(NH_4)_6Mo_7O_{24}·4H_2O$, 0.014 mmol		8:1:16:1	pink needles **2**
2	$CoF_2·4H_2O$, 0.40 mmol	$(NH_4)_6Mo_7O_{24}·4H_2O$, 0.014 mmol		4:1:8:1	pink powder (**2**) without monocrystalline phase
3	$CoF_2·4H_2O$, 0.80 mmol	MoO_3, 0.10 mmol		8:1:16:1	two phases, pink crystals **2** (major) and colorless polycrystals (minor) ~70:30
4	$CoF_2·4H_2O$, 0.80 mmol	MoO_3, 0.10 mmol	NH_4F, 0.086 mmol	8:1:16.9:1	two phases, pink crystals **2** and colorless polycrystals ~70:30
5	$CoF_2·4H_2O$, 0.80 mmol	MoO_3, 0.10 mmol	HF (7%), 0.72 mmol	8:1:23.2:1	two phases, white powder (major) and orange prisms **3** (~80:20%)[b]
6	$Co(OAc)_2·4H_2O$, 0.80 mmol	MoO_3, 0.10 mmol	HF (7%), 0.72 mmol	1:2:7.2:1	two phases, white powder and orange prisms **3** in close proportions
7	$Co(OAc)_2·4H_2O$, 0.80 mmol	MoO_3, 0.10 mmol	HF (22%), 2.89 mmol	1:2:28.9:1	two phases, white powder and orange prisms **3** (~90:10%)[b]
8	$Co(OAc)_2·4H_2O$, 0.80 mmol	MoO_3, 0.10 mmol	HF (50%), 5.78 mmol	1:2:57.8:1	white powder
9	$Co(OAc)_2·4H_2O$, 0.80 mmol	MoO_3, 0.10 mmol	NH_4F and HF (7%), 0.086 mmol and 0.72 mmol	1:2:8.1:1	two phases, white powder and orange prisms **3** in similar quantities
10	$Co(OAc)_2·4H_2O$, 0.80 mmol	$(NH_4)_6Mo_7O_{24}·4H_2O$, 0.0284 mmol	HF (7%), 0.72 mmol	1:2:7.2:1	two phases, white slurry and orange prisms **3** (trace amount)

[a]Temperature regime: held at 130 °C for 36 h, cooling to rt for 48 h, and kept at rt for 48 h prior to analysis. [b]Isolated yield after $CHBr_3/CHCl_3$ separation.

to the choice of organic ligands with geometric and electronic characteristics that allow intelligent control over the secondary building units (SBUs) of a desirable configuration and their charge and spatial distributions in the crystal lattice.

Being aware that neutral 1,2,4-tr-derivatives have a tendency to form a variety of discrete multicharged cationic clusters,[9] like linear $[M_3(N1,N2\text{-tr})_6]^{6+}$, where M = low-valent late-transition metal cations, for example, Fe^{II} or Co^{II},[10] we selected a simple bitopic ligand, 1,3-bis(1,2,4-triazol-4-yl)propane (tr_2pr), as a very versatile candidate for the construction of 3D coordination solids with potential ability to incorporate large molybdenum oxide fluoride polyanions. The ligand flexibility, here introduced through a propylene linkage, can be regarded as an advantageous factor for "fine-tuning" the cavity/open-channel sizes in the framework, and generally it can lead to diverse structural motifs.

EXPERIMENTAL SECTION

Caution! *Hydrofluoric acid, HF, is toxic and corrosive and must be handled in a well-ventilated fume hood with extreme caution using appropriate protective gear.*

All chemicals were of reagent grade and used as received without further purification. The 1,3-bis(1,2,4-triazol-4-yl)propane ligand (tr_2pr) was synthesized in 33% yield by refluxing of propane-1,3-diamine with *N*,*N*-dimethylformamide azine in toluene in the presence of *p*-toluenesulfonic acid monohydrate as the catalyst.[11]

Synthesis of the Coordination Compounds. Complexes **1**–**3** were prepared using hydrothermal techniques in the following way.

*$[Mo_2F_2O_5(tr_2pr)]$ (**1**).* A mixture of $Co(OAc)_2·4H_2O$ (24.9 mg, 0.1 mmol), tr_2pr (17.8 mg, 0.1 mmol), and MoO_3 (28.8 mg, 0.2 mmol) in a 1:1:2 molar ratio were placed in a 20 mL Teflon-lined autoclave. Then, 5 mL of water and 100 μL of 22% HF (1.18 mmol) aqueous solution were added to the solids. The reactor was sealed and heated to 160 °C in an oven equipped with a programmable temperature controller. After 36 h heating, the vessel was slowly cooled to rt within 60 h affording a white powdered precipitate. The mother liquor was decanted from the solid. Evaporation of the solution at rt yielded colorless prisms of the desired product after 2 weeks (11.0 mg, 22%). Anal. Calcd for $C_7H_{10}F_2Mo_2N_6O_5$: C, 17.23; H, 2.07; N, 17.22. Found: C, 17.14; H, 2.00; N, 17.18. The white precipitate consists of an unknown crystalline phase (Anal. Found: C, 19.32; H 3.22; N, 18.88; see also XRPD patterns, Figure S16, Supporting Information). Similar results were observed when the reaction proceeded at HF/Mo ratios of 15:1 or even higher.

*$[Co_3(tr_2pr)_2(MoO_4)_2F_2]·7H_2O$ (**2**).* A mixture of $CoF_2·4H_2O$ (135 mg, 0.799 mmol), tr_2pr (17.8 mg, 0.1 mmol), $(NH_4)_6Mo_7O_{24}·4H_2O$ (17.6 mg, 0.0142 mmol), and 5 mL of water (molar ratio $Co^{II}/Mo^{VI}/F^-/tr_2pr$ = 8:1:16:1) was intensively stirred at rt for a few minutes in a 20 mL Teflon-lined autoclave before being sealed. The autoclave was heated up to 130 °C, held for 36 h, and gradually cooled at 2.1 °C/h to rt and then left undisturbed for 2 days. The monophase pink needles were isolated in 42.0 mg yield (83%). Anal. Calcd for $C_{14}H_{34}Co_3F_2Mo_2N_{12}O_{15}$: C, 16.53; H, 3.37; N, 16.52. Found: C, 16.59; H, 3.36; N, 16.58. IR (KBr discs, selected bands, cm^{-1}): 638s, 688m, 754s, 822s, 858s, 908s, 1008m, 1046m, 1082s, 1210s, 1248m, 1284m, 1322w, 1402m, 1452m, 1490m, 1550s, 1652m, 2834m, 2892m, 3008s, 3080s, 3374s.

*$[Co_3(H_2O)_2(tr_2pr)_3(Mo_8O_{26}F_2)]·3H_2O$, (**3**).* A mixture of $Co(OAc)_2·4H_2O$ (24.9 mg, 0.1 mmol), tr_2pr (17.8 mg, 0.1 mmol), and MoO_3 (28.8 mg, 0.2 mmol) in 5 mL of water and 200 μL of 7% HF (0.72 mmol) aqueous solution (molar ratio $Co^{II}/Mo^{VI}/F^-/tr_2pr$ = 1:2:7:1) was heated in a Teflon-lined autoclave at 130 °C. After 36 h, the reaction vessel was slowly cooled at 2.1 °C/h to rt and then left undisturbed for 2 days. The resultant reaction mixture contained a white powder of a Co-free solid as a major phase and orange prismatic crystals of the desired product. The crystals of **3** were separated from the white powder in a $CHBr_3/CHCl_3$ solvent mixture based on their different density (~2.30 g cm^{-3} for the white precipitate vs ~2.70 g cm^{-3} for **3**) and by sonication in propanol-2 and in water (Figure S13, Supporting Information). In this way, compound **3** was isolated in 37% yield (18.6 mg), based on Mo. Anal. Calcd for $C_{21}H_{40}Co_3F_2Mo_8N_{18}O_{31}$: C, 12.47; H, 1.99; N, 12.46. Found: C, 12.43; H, 2.09; N, 12.48. IR (KBr discs, selected bands, cm^{-1}): 470s, 488s, 536s, 570s, 630s, 674s, 692s, 782m, 858s, 896s, 934s, 1014w, 1052s, 1088s, 1220s, 1282w, 1324w, 1360w, 1404m, 1452m, 1464m,1492w, 1560s, 1626m, 2890m, 2960m, 3024m, 3064s, 3114m, 3142m, 3340m, 3340m, 3440m.

The attempts to optimize the reaction by increasing the reaction temperature (160 °C) and by changing reactant sources ($Co(OAc)_2·4H_2O$ vs $CoF_2·4H_2O$ and MoO_3 vs $(NH_4)_6Mo_7O_{24}·4H_2O$), as well as their ratios, did not improve the yield of the product.

Synthesis. Exploring the hydrothermal reactions that afforded three new fluorinated hybrid solids, **1**–**3**, we systematically changed many synthetic parameters. The corresponding data as reactant ratios,

dx.doi.org/10.1021/ic400954x | Inorg. Chem. 2013, 52, 8784–8794

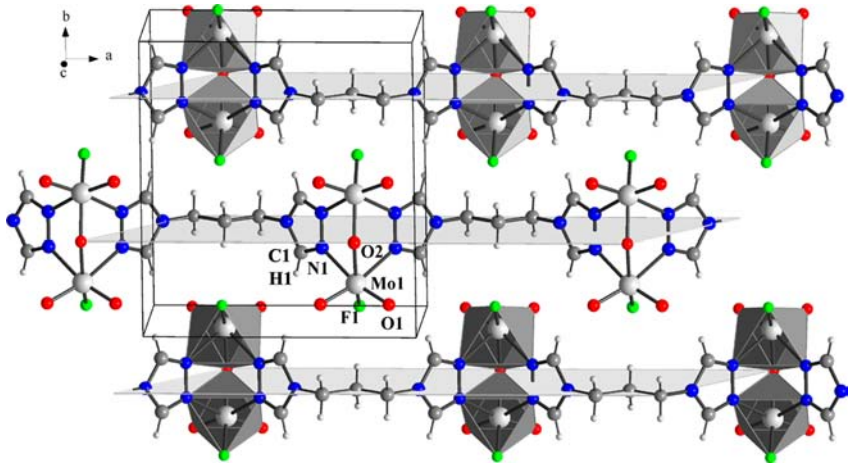

Figure 1. Formation of a zigzag chain structure in compound **1** (Mo1−N1 2.343(3), Mo1−O2 1.9030(16), Mo−O1 1.696(3), Mo1−F1 1.917(3) Å).

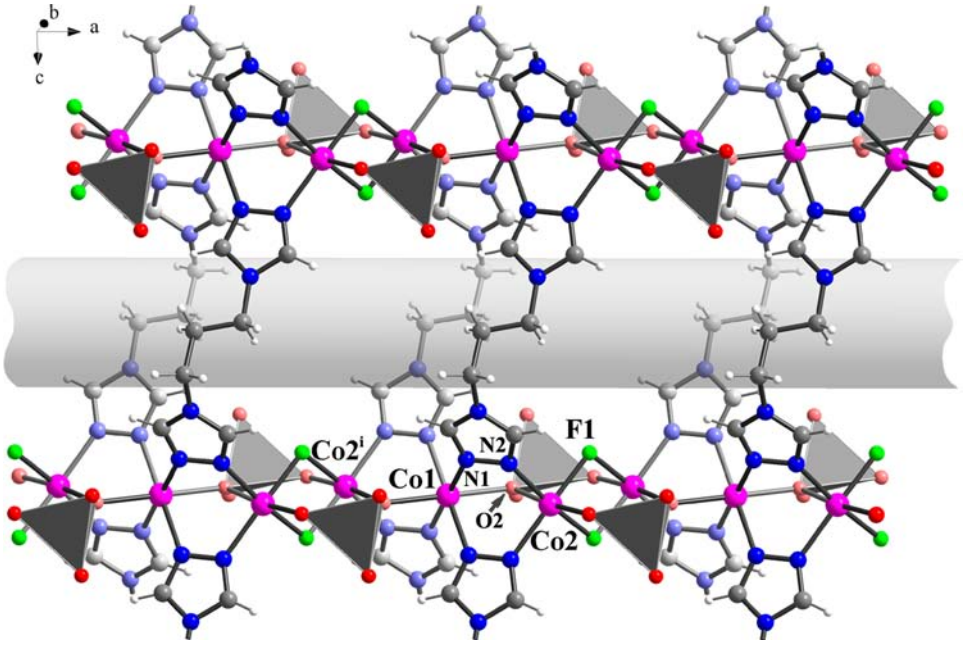

Figure 2. The $[Co_3(\mu_3\text{-}MoO_4)_2(\mu_2\text{-}F)_2]$ inorganic chains are interlinked by tr_2pr into an extended layered motif for **2**, with open channels running along the *a* axis. Color legend: fluoride, green; carbon, gray and light-gray; nitrogen, blue and light-blue; hydrogen, white; oxygen, red and light-red (MoO_4^{2-} are shown as dark- and light-gray polyhedra). Symmetry code: (i) $-x + 1, -y + 1, -z + 1$.

temperature regime, and some trends in the compound formation are summarized in Table 1. $Co(OAc)_2{\cdot}4H_2O/CoF_2{\cdot}4H_2O$ and $MoO_3/(NH_4)_6Mo_7O_{24}{\cdot}4H_2O$ were selected as Co^{II} and Mo^{VI} precursors, respectively, while the F^- content in solutions was adjusted by addition of aqueous HF, NH_4F, or CoF_2. Powder X-ray diffraction and crystal habit were used to identify the reaction products and to confirm their purity.

First, in acidic solution and at a high molar ratio of the HF/Mo^{VI} source (∼6:1 or higher at 160 °C), the Co-free compound $[Mo_2F_2O_5(tr_2pr)]$ (**1**) was isolated and characterized, whereas a lowering of the HF concentration and the HF/Mo^{VI} ratio to ∼3.6:1 in a mild temperature regime (130 °C) was favorable for the condensation of fluorooctamolybdate anions $[Mo_8O_{26}F_2]^{6-}$, which were incorporated into the Co^{II}-containing metal−organic framework **3**. In these two cases, the addition of HF to the starting reactants is essential, and thus, the formation of **1** and **3** is mainly dependent upon the HF concentration and the HF/Mo^{VI} ratio. As evidenced in Table 1 (entry 1), a large excess of fluoride ions, as well as Co^{II}, was necessary for the crystallization of a pure phase of the mixed-anion complex **2**, prepared in high yield. However, no crystalline product of **2** was obtained in the presence of even a tiny amount of HF, suggesting its low stability in acids (entry 5). That is the reason the formation of a crystalline phase **2** under hydrothermal conditions, usually running at low pH, requires a large excess of Co^{II}. A series of experiments proceeding at high temperature (160 °C) showed a noticeable decline in product yields (**2** and **3**). We also found that the choice of Mo^{VI} precursors is more sensitive for the preparation of compound **3** versus complex **2**.

These observations suggest that the acidity of the reaction medium, the concentration of fluoride anions and the HF/Mo^{VI} ratio are key factors that predetermine the formation of condensed oxyfluoro di/octamolybdate (**1**, **3**), while for the mixed-anion fluoride/molybdate species (**2**), a high excess of Co^{II} is required.

Measurements. Elemental analysis was carried out with a Vario EL-Heraeus microanalyzer. IR-spectra (400−4000 cm^{-1}) were collected using a Perkin-Elmer FTIR spectrometer on KBr discs. The X-ray powder diffraction was carried out on a Stoe STADIP (Cu $K\alpha_1$) using a linear PSD detector. The temperature-dependent X-ray

dx.doi.org/10.1021/ic400954x | *Inorg. Chem.* 2013, 52, 8784−8794

Table 2. Principal Geometric Parameters of $[Co_3(\mu_2\text{-tr})_2(\mu_3\text{-}MoO_4)_2(\mu_2\text{-F})_2]$, $[Co_3(\mu_2\text{-tr})_6]^{6+}$, and μ_4-$[Mo_8O_{26}F_2]^{6-}$ Observed in the Crystal Structures of 2 and 3

compound	2		3	
$\{Co\}_3$-fragment	"central Co" Co1	"terminal Co" Co2	"central Co" Co1 and Co3	"terminal Co" Co2 and Co4
coord. environment	$\{N_4O_2\}$	$\{N_2O_2F_2\}$	$\{N_6\}$	$\{N_3O_3\}$
Co−N, N^1,N^2-tr	2.122(5), 2.123(5)	2.083(5), 2.105(5)	2.107(3)−2.167(3), 2.118(3)−2.153(3)	2.068(3)−2.098(3), 2.076(3)−2.098(3)
Co−F		2.041(3), 2.057(3)		
$Co-O_{(water)}$				2.161(3) and 2.154(2)
Co−O ($[MoO_4]^{2-}$)	2.104(4)	2.054(4), 2.159(4)		
Co−O ($[Mo_8O_{26}F_2]^{6-}$)				2.098(3)−2.131(2), 2.055(2)−2.061(2)
Co···Co	3.3596(7) (intracluster), 3.0709(15) (intercluster)		3.8028(4), 3.8236(4) (intracluster)	

$[Mo_8O_{26}F_2]^{6-}$ in 3[a]

Mo−F	Mo3−F1b	1.822(2)	Mo7−F2	1.977(2)
$Mo-O_{(terminal,coordinating)}$	Mo1−O4	1.736(2)	Mo5−O16	1.735(2)
	Mo1−O3	1.736(2)	Mo5−O17	1.735(2)
$Mo-O_{(terminal,noncoordinating)}$	Mo2−O5	1.697(2)	Mo6−O18	1.704(2)
	Mo3−O6	1.697(2)	Mo7−O19	1.703(3)
	Mo3−O7a[b]	1.828(2)	Mo7−O20	1.721(3)
	Mo4−O8	1.701(2)	Mo8−O22	1.710(2)
	Mo4−O9	1.729(2)	Mo8−O21	1.716(2)
Mo−O{μ_2-O}	Mo3−O11	2.080(2)	Mo5−O24	1.910(2)
	Mo1−O15	1.991(2)	Mo5−O28	2.308(2)
	Mo4−O15	1.891(2)	Mo6−O28	1.744(2)
	Mo1−O11i	1.836(2)	Mo7−O27	1.903(2)
	Mo2−O10	1.749(2)	Mo8−O27	1.939(2)
	Mo4−O10i	2.364(2)	Mo8−O24	1.953(2)
Mo−O{μ_3-O}	Mo1−O12i	2.355(2)	Mo5−O23	1.893(2)
	Mo2−O12	1.875(2)	Mo6−O26	1.890(2)
	Mo2−O13	2.200(2)	Mo6−O23vii	2.133(2)
	Mo3−O12	2.201(2)	Mo7−O23vii	2.189(2)
	Mo4−O13	1.955(2)	Mo7−O26	2.206(2)
	Mo3−O13	2.010(2)	Mo8−O26	2.285(2)
Mo−O{μ_4-O}	Mo1−O14	2.189(2)	Mo5−O25	2.180(2)
	Mo2−O14	1.946(2)	Mo6−O25vii	1.953(2)
	Mo2−O14i	2.451(2)	Mo6−O25	2.537(2)
	Mo4−O14	2.241(2)	Mo8−O25	2.262(2)

[a]Symmetry codes: (i) $-x+1, -y+1, -z+1$; (vii) $-x, -y, -z$. [b]Involved in strong H-bonding interaction, O7a···H−O2 (x, $1+y$, z), 2.799(3)Å.

measurements were carried out on a Stoe STADIP with a high-temperature attachment and image plate detector system. Thermogravimetric/differential thermal analysis mass spectrometry (TG/DTA-MS) was carried out on a Netzsch F1 Jupiter device connected to an Aeolos mass spectrometer. The sample was heated at a rate of 10 K min^{-1}. Magnetic susceptibility measurements were made on a Quantum Design MPMS SQUID-*XL* magnetometer under an applied magnetic field of 10^3 Oe between 300 and 1.9 K. The samples were prepared in a gelatin capsule. Diamagnetic corrections were made for the samples using the approximation $-0.45 \times$ molecular weight $\times 10^{-6}$ cm^3 mol^{-1}, and the sample holder was corrected for by measuring directly the susceptibility of the empty capsule.

X-ray Crystallography. Diffraction data were collected at 296 K on a Bruker APEXII CCD area-detector diffractometer (φ scans) (graphite-monochromated Mo Kα radiation, $\lambda = 0.71073$ Å). The data were corrected for Lorentz-polarization effects and for the effects of absorption (multiscans method). The structures were solved by direct methods and refined by full-matrix least-squares on F^2 using the SHELX-97 package.[12]

Crystallographic data and experimental details for structural analyses are summarized in Table S1, Supporting Information. The crystallographic material can also be obtained from the CCDC, the deposition numbers being CCDC 934152−934154.

CRYSTAL STRUCTURES

The asymmetric unit of compound **1** consists of only one-fourth of tr_2pr, one molybdenum, one fluorine, and two oxygen atoms. The Mo atom possesses a distorted octahedral environment completed by two N(tr) atoms in *cis* positions, a μ_2-bridging oxygen, a terminal fluorine, and two *cis*-orientated "molybdenyl" oxygen atoms (Figure 1). Two molybdenums are joined into a dinuclear unit through a bridging O2 atom as a common vertex, whereas two triazolyl-groups serve as a short double-link between the Mo centers (Mo···Mo 3.574(1) Å). The tr_2pr ligand contains a linear aliphatic $-(CH_2)_3-$ spacer between tr-termini suggesting the existence of conformational flexibility similar to that described for the glutarate anion: *anti*−*anti*, *anti*−*gauche*, and *gauche*−*gauche*.[13] In **1**, tr_2pr adopts an *anti*−*anti* conformation type that provides a 10.733(1) Å distance for the interconnection between the dinuclear $[Mo_2F_2O_5(tr)_2]$ units, predetermining a more favorable 1D zigzag motif,[14] running along the *a* axis.

The 2D crystal structure of the mixed-anion complex **2** consists of centrosymmetric trinuclear $[Co_3(\mu_2\text{-tr})_4(\mu_3\text{-}MoO_4)_2(\mu_2\text{-F})_2]$ fragments that can be regarded as elementary repeating units self-assembling in the Co(II)-containing undulating chains (Figure 2). The "inner" cluster configuration

dx.doi.org/10.1021/ic400954x | Inorg. Chem. 2013, 52, 8784−8794

is strongly supported by four μ_2-tr and one μ-MoO_4^{2-} bridges, whereas the interconnection between the neighboring clusters is supplied by quadruple bridges of μ-(O1,O2)-MoO_4^{2-} and F^- anions in a ratio of 1:1. The unique binding combinations of organic/inorganic pairs adjust relatively short intrachain distances between adjacent Co(II) centers (3.3596(7) Å for the triple-bridging [Co-$(tr)_2(MoO_4)$-Co] and 3.0709(15) Å for quadruple-bridging [Co-$(F)_2(MoO_4)_2$-Co] units) (Table 2). Such cooperative interactions of fluoride and tetrahedral oxoanions seem to be a quite rare example, which however is extremely important in the structural chemistry of organically templated vanadium and iron fluoroarsenates (F^-/AsO_4^{3-} or $HAsO_4^{2-}$)[15,16] and mixed-valent iron fluorophosphates.[17] Similarly to complex **1**, the tr_2pr ligand serves as a tetradentate donor interlinking the neighboring inorganic chains [$Co_3(\mu_3$-$MoO_4)_2(\mu_2$-$F)_2$] into layer motifs. However, the presence of a bent ligand conformation, *gauche*−*anti*, illustrated by the torsion angles N3−C5−C6−C7 = −75.3(7)° and C5−C6−C7−N6 = −169.3(5)°, results in the formation of open channels with a van der Waals cross-section of 1.5 Å × 4 Å running through the layers along the *a* axis (Figure 3). Water molecules reside inside the channels and within the interlayer space occupying a total solvent accessible volume of 164 Å^3 (or 21% of the unit cell).[18]

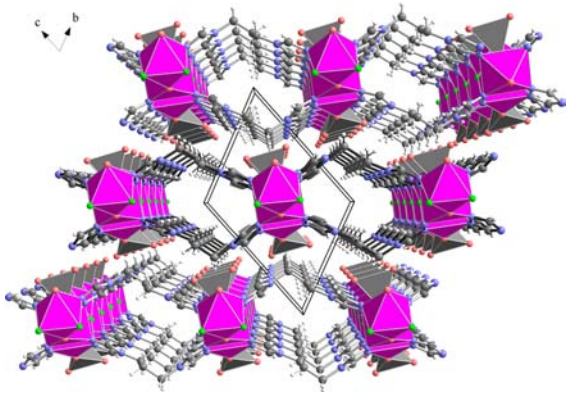

Figure 3. The {[$Co_3(tr_2pr)_2(MoO_4)_2F_2$]} stacked layers in the crystal structure of **2** leaving rhombic channels in which guest water molecules (not shown) are accommodated. Color legend: fluoride, green; carbon, gray; nitrogen, light-blue; hydrogen, white; oxygen, light-red; MoO_4^{2-} tetrahedra are shown in gray, and Co(II)-centered octahedra are shown in purple.

In complex **3**, the asymmetric unit of the crystal contains two half-$\{Co_3\}^{6+}$ clusters, two half-$[Mo_8O_{26}F_2]^{6-}$ anions, three tr_2pr, and two coordinating and three noncoordinating water molecules (Figure 4, Table 2). The $\{Co_3\}^{6+}$ basic building units consist of two crystallographically independent Co atoms, which are aligned in a linear sequence utilizing six μ_2-tr groups, for example, a triple-bridge pair. The connection mode determines the 3.8028(4) and 3.8236(4) Å separation of Co3···Co4 and Co1···Co2 atoms, respectively. The discrete motif is a very common case in the coordination chemistry of 1,2,4-triazolyl ligands.[9] The central Co atom in the $\{N_6\}$ environment is located on an inversion center, whereas the terminal atoms possess distorted $\{N_3O_3\}$ octahedra, which are completed by coordination of a water molecule and [μ_4-$Mo_8O_{26}F_2]^{6-}$ anions.

The geometric configuration of the molecular difluorooctamolybdate $[Mo_8O_{26}F_2]^{6-}$ anion can be imagined as derived

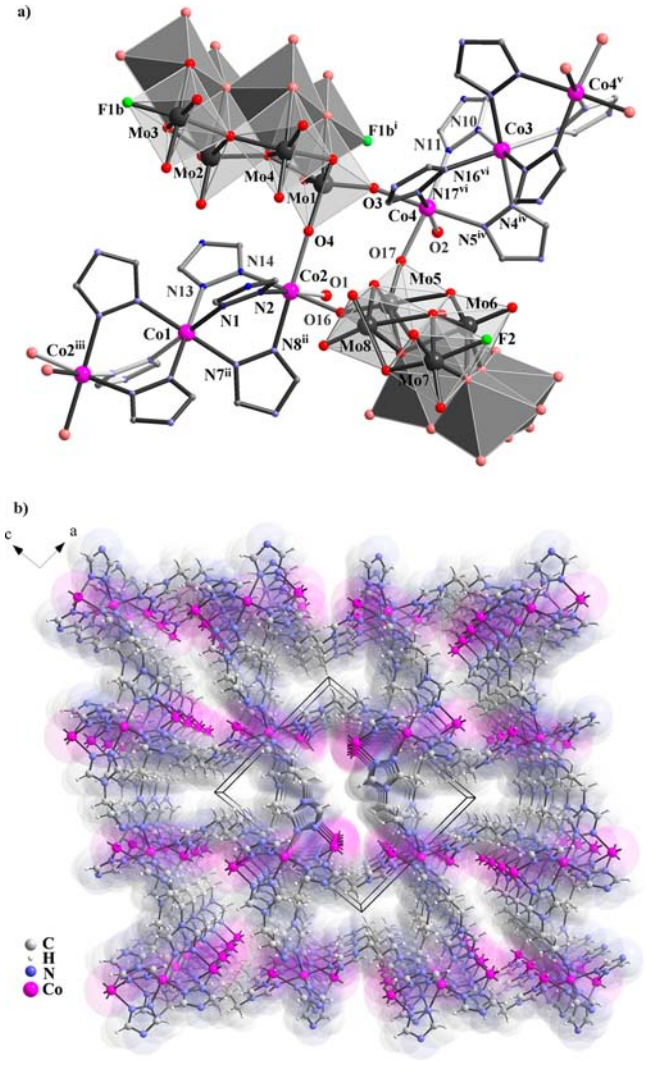

Figure 4. (a) The representation includes the asymmetric unit of [$Co_3(H_2O)_2(tr_2pr)_3(Mo_8O_{26}F_2)$]·$3H_2O$ (**3**) with the crystallographically different but chemically identical two half-$\{Co_3\}$clusters and two half-$[Mo_8O_{26}F_2]^{6-}$ units. (b) Perspective view showing the 3D [$Co_3(tr_2pr)_3$] cationic framework with open channels. Symmetry codes: (i) $-x+1, -y+1, -z+1$; (ii) $x, y, z-1$; (iii) $-x+1, -y+1, -z$; (iv) $x, y-1, z$; (v) $-x, -y, -z+1$; (vi) $-x+1, -y, -z+1$; (vii) $-x, -y, -z$.

from the γ-$[Mo_8O_{26}]^{4-}$ platform.[19] Six Mo atoms in distorted [MoO_6] octahedra and two in distorted [MoO_5F] environments are joined through an edge-sharing junction mode.

Due to the Co(II) octahedral environments, the radial arrangement of six triazolyl arms around the trinuclear cluster affords their direction toward the vertices of a virtual square bipyramid. The organic ligands act as uniform tetradentate donors, which, quite unexpectedly, display different conformations, *anti*−*anti* and *anti*−*gauche* in a 2:1 ratio. The $[Co_3(tr)_6]^{6+}$ units, acting as nodes, are connected with distances ranging from 10.72 to 12.45 Å into a primitive cubic network (α-Po type). The framework occupies almost half of the overall volume of the crystal structure, calculated with the PLATON program.[18] The open channels with different cross sections and a maximum value of ∼2 Å × 7 Å, including van der Waals distances, are distributed along the crystallographic axes and contain $[Mo_8O_{26}F_2]^{6-}$ anions and water molecules. Apparently, the charge-compensating ($[Co_3(tr)_6]^{6+}$ vs $[Mo_8O_{26}F_2]^{6-}$) and

dx.doi.org/10.1021/ic400954x | Inorg. Chem. 2013, 52, 8784−8794

space-filling (or shape complementary) role of difluorooctamolybdate anions is enhanced by its tetradentate binding mode (Figure 5) (Co−O{Mo_8} 2.0575(2)−2.131(2) Å). In this case,

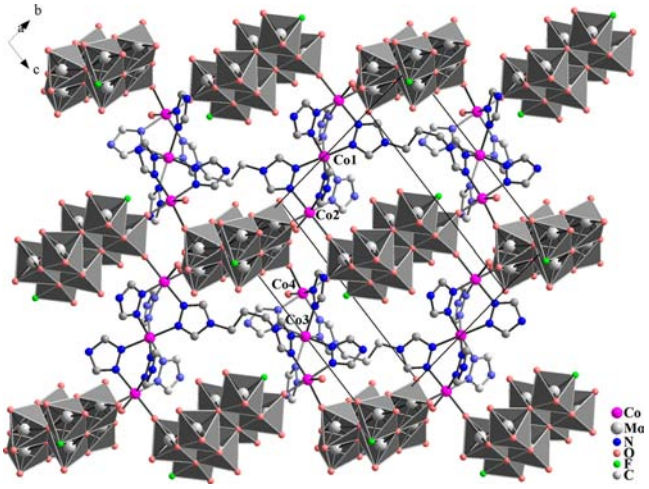

Figure 5. Projection of the structure of $[Co_3(H_2O)_2(tr_2pr)_3(Mo_8O_{26}F_2)]\cdot 3H_2O$ (**3**) along the $[\bar{3}10]$ axis. The $[Mo_8O_{26}F_2]^{6-}$ anions adopt a tetradentate bridging mode and interlink $[Co_3(tr)_6]$ SBUs into a layer motif through peripheral Co atoms.

each $[Mo_8O_{26}F_2]^{6-}$ anion serves as a tetratopic connector that in combination with the $\{Co\}_3$ nodes leads to a novel type of a two-nodal 4,10-c net having a Schläfli point symbol of $\{3^2.4^3.5\}\{3^4.4^{20}.5^{16}.6^5\}$.[20] Unlike the dinuclear $\{Mo_2F_2O_5(tr)_2\}$ units in complex **1**, the $[Mo_8O_{26}F_2]^{6-}$ oxofluoride species form a rich set of characteristic H-bonding interactions (O−H···O, C−H···O, etc.), which involve coordinating and noncoordinating water molecules, triazolyl fragments, and even linker C−H protons (see Supporting Information).

QUANTUM CHEMICAL CALCULATIONS

The geometry of the $[Mo_8O_{26}F_2]^{6-}$ anion was optimized with density functional theory using approaches previously tested and shown to reproduce the structures and spectroscopic properties of iso- and heteropolymolybdates.[21] All calculations were performed with the molecular ADF program, version 2012.[22] Functionals based on the Vosko−Wilk−Nusair (VWN) form of the local density approximation have previously been shown[21] to reproduce the structures of polyanions and were employed here. In addition, calculations were also performed at the GGA level using BP86 and at the meta-GGA level using the M06-L functional to improve the description of the weak interactions. Slater-type orbital basis sets of triple-ζ quality were employed using frozen cores (in ADF; O 1s, F 1s, and Mo 3d) for the VWN calculations. For the M06-L calculations, full electron basis sets were used. In all calculations, relativistic effects were incorporated using the spin-free zeroth-order regular approximation (scalar ZORA).[23] Interactions with the environment are important for this highly charged anion, and this was modeled through use of a water solvent model using the COSMO approach available in ADF.[24] Bond order and related calculations were carried out using the methods previously applied to isopolyanions and other transition metal complexes.[25]

Table 3 details the key geometrical parameters for the $[Mo_8O_{26}F_2]^{6-}$ anion obtained using these approaches. The VWN approach has previously been shown to lead to reproduce the crystallographically determined structures of polyoxometalates, including those of the octamolybdates,[26] reasonably well when applied to isolated anions, a consequence of the tendency of this approach to overbind compensating for

Table 3. The Principal Geometric Parameters (in Å) in the Optimized Structure of $[Mo_8O_{26}F_2]^{6-}$

			VWN	VWN/COSMO	BP86/COSMO	M06-L/COSMO
Mo−F	Mo3−F1b	Mo7−F2	2.04	1.94	1.99	1.96
$Mo-O_{(terminal,coordinating)}$	Mo1−O4	Mo5−O16	1.74	1.72	1.74	1.72
	Mo1−O3	Mo5−O17	1.73	1.72	1.74	1.72
$Mo-O_{(terminal,noncoordinating)}$	Mo2−O5	Mo6−O18	1.72	1.71	1.73	1.71
	Mo3−O6	Mo7−O19	1.72	1.71	1.73	1.71
	Mo3−O7a	Mo7−O20	1.73	1.73	1.75	1.72
	Mo4−O8	Mo8−O22	1.73	1.72	1.74	1.72
	Mo4−O9	Mo8−O21	1.73	1.72	1.74	1.72
Mo−O{μ_2-O}	Mo3−O11	Mo5−O24	1.91	1.99	2.03	2.10
	Mo1−O15	Mo5−O28	1.93	1.97	2.01	2.06
	Mo4−O15	Mo6−O28	1.91	1.87	1.90	1.87
	Mo1−O11i	Mo7−O27	1.93	1.87	1.89	1.85
	Mo2−O10	Mo8−O27	1.76	1.77	1.77	1.76
	Mo4−O10i	Mo8−O24	2.25	2.24	2.40	2.35
Mo−O{μ_3-O}	Mo1−O12i	Mo5−O23	2.11	2.23	2.29	2.32
	Mo2−O12	Mo6−O26	1.86	1.86	1.87	1.87
	Mo2−O13	Mo6−O23vii	2.24	2.15	2.28	2.20
	Mo3−O12	Mo7−O23vii	2.54	2.30	2.42	2.10
	Mo4−O13	Mo7−O26	1.99	1.97	1.99	2.02
	Mo3−O13	Mo8−O26	1.98	1.96	1.96	1.94
Mo−O{μ_4-O}	Mo1−O14	Mo5−O25	2.51	2.26	2.33	2.28
	Mo2−O14	Mo6−O25vii	1.91	1.93	1.95	1.96
	Mo2−O14i	Mo6−O25	2.41	2.35	2.48	2.38
	Mo4−O14	Mo8−O25	2.18	2.21	2.23	2.23

dx.doi.org/10.1021/ic400954x | Inorg. Chem. 2013, 52, 8784−8794

Table 4. Bond Orders in (a) MoF_6, $[MoOF_5]^-$, *cis*-$[MoO_2F_4]^{2-}$, and *fac*-$[MoO_3F_3]^{3-}$ and (b) $[Mo_8O_{26}F_2]^{6-}$

(a) MoF_6, $[MoOF_5]^-$, *cis*-$[MoO_2F_4]^{2-}$, and *fac*-$[MoO_3F_3]^{3-}$			
	Mo−F_{trans}	Mo−F_{cis}	Mo−O
MoF_6	0.86 (0.32σ and 2 × 0.27π)		
$[MoOF_5]^-$	0.74 (0.38σ and 2 × 0.18π)	0.76	2.01 (0.72σ and 2 × 0.65π)
cis-$[MoO_2F_4]^{2-}$	0.62 (0.08π)	0.66	1.71 (0.29π)
fac-$[MoO_3F_3]^{3-}$	0.50		1.61

(b) $[Mo_8O_{26}F_2]^{6-}$					
	Mo−F	Mo−$O_{(terminal)}$	Mo−O{μ_2-O}	**Mo−O{μ_3-O}**	**Mo−O{μ_4-O}**
$[Mo_8O_{26}F_2]^{6-}$	0.54	1.58−1.61	1.27, 0.70−0.71	0.24−0.49	0.18−0.28

the lack of counterion stabilization. Comparison of the Mo−F and Mo−O bond lengths obtained using this approach for $[Mo_8O_{26}F_2]^{6-}$ with the crystallographic values in Table 2 shows reasonable agreement except for the bonds involving Mo3 and Mo7 (i.e., the metal atoms which are attached to fluoride). For these octahedra, the VWN calculation predicts a somewhat longer Mo−F bond than is observed and a smaller *trans* influence for fluoride and a larger *trans* influence for the terminal oxo groups. The Mo1−O14 bond is predicted at this level to lengthen to over 2.5 Å so that the octahedron involving Mo1 is highly distorted. Inclusion of a solvent model in the VWN/COSMO calculations, to account for the H-bonding interactions, and improvement of the density functional, in the BP86 and M06-L calculations, improves the agreement, with the Mo−F bond length reduced by around 5%. The optimized structure at all levels is much more symmetric than that in the crystal environment. The sensitivity of the Mo−F bond and the associated $\{MoFO_5\}$ unit to the environment is clear from the difference in the optimized structures obtained with and without solvent and in the structures of this unit in the two polyanions in the unit cell. These results suggest that the gas-phase VWN approach is less suitable for the study of oxyfluorides than it is for oxoanions. The more ionic character of the Mo−F bond and the relatively high charge of this particular anion appear to require a higher level treatment.

The bonding in oxyfluorides and oxyanions has been investigated previously.[21,26,27] Strong mixing between the empty d-orbitals on the central transition metal cation and the oxide *p*-orbitals leads to the formation of short and strong terminal metal−oxide bonds, which lead to a weakening of the bonds to the *trans* oxide anions. As a result, there are significant distortions of the $\{MO_6\}$ and $\{MO_xF_{6-x}\}$ octahedra with movement of the cation toward the terminal oxo groups. Table 4 lists calculated bond orders for the model systems MoF_6, $[MoOF_5]^-$, *cis*-$[MoO_2F_4]^{2-}$, and *fac*-$[MoO_3F_3]^{3-}$. For the first three of these, the symmetry allows an insight into the relative importance of the σ and π bonding. Both Mo−O and Mo−F bonds are best described as being polar multiple bonds in these systems. The covalent Mo−F bond in MoF_6 is a little less than a full single bond, but this is made from contributions that are roughly (1/3)σ and (2/3)π. Similarly, the Mo−O bond in $[MoOF_5]^-$ is a double bond made up of contributions that are also roughly (1/3)σ and (2/3)π. The higher multiplicity of the Mo−O bond naturally reflects the higher valency of oxygen. As x increases in the $[MoO_xF_{6-x}]^{x-}$ systems, the Mo−F bond order is reduced with the influence of the O atom being greater when it is located *trans* to F. This influence appears to be greater for the π component of the Mo−F bond.

In polyanions, the large *trans* influence of the terminal Mo−O bonds leads to the trans-located bonds being relatively long and weak. The O atoms involved in these weak bonds satisfy their valencies through the formation of bonds to multiple Mo atoms[26] leading to bridging Mo−O−Mo groups and polymerization. Table 4 also contains a summary of the bond orders in $[Mo_8O_{26}F_2]^{6-}$. Figure 6a shows how the bond order depends on the Mo−O bond length in this anion and in the octamolybdates. In the $[Mo_8O_{26}F_2]^{6-}$ anion, the bond orders for the terminal Mo−O bonds are very similar for the $\{MoO_6\}$ and $\{MoO_5F\}$ octahedra. The Mo−O {μ_2-O} bonds appear to form two sets. O10 makes one short (1.75 Å) and one long (2.36 Å) bond. The former is only slightly longer than those of the Mo−$O_{(terminal)}$ bonds. The bond orders confirm that this

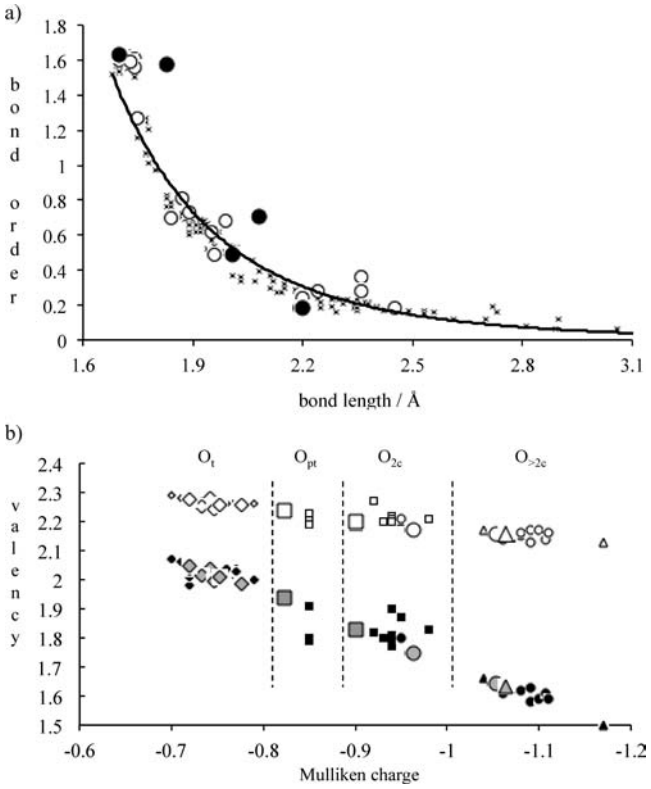

Figure 6. Variation of (a) bond order with bond length and (b) oxygen covalency (shaded) and full valency (open) with Mulliken charges for the isomers of octamolybdate and $[Mo_8O_{26}F_2]^{6-}$. In panel a, the values for $[Mo_8O_{26}F_2]^{6-}$ are shown as large circles with the shaded circles representing the Mo−O bonds in the $\{MoO_4F_2\}$ octahedra. In panel b, the oxygen atoms are labeled by their coordination numbers as terminal (◇), μ_2 (□), μ_3 (○), and {μ_4, μ_5} (△). The filled circles represent covalencies, and the open circles represent total valencies. The values for $[Mo_8O_{26}F_2]^{6-}$ are shown as larger symbols.

dx.doi.org/10.1021/ic400954x | *Inorg. Chem.* 2013, 52, 8784−8794

oxygen atom might be considered to be a pseudoterminal type, as seen in the octamolybdates.[26]

The Mo−$O_{(terminal)}$ bonds appear to be similar in the $\{MoO_6\}$ and $\{MoO_5F\}$ octahedra. Comparison with the bond orders found in the octamolybdates in Figure 6a suggests that the two Mo−$O_{(terminal)}$ bonds in the $\{MoO_5F\}$ octahedra behave very similarly to type II *cis*-dioxo groups, that is, the presence of a fluoride ion is electronically quite similar to that of a μ_2-O ion, except that some lengthening of the terminal bonds occurs.

In the octamolybdates and in other molybdates,[26] it has previously been shown that the different types of oxygen atoms can usefully be characterized using their total covalency (the sum of the covalent bond orders) and total valencies (the sum of their covalent and electrostatic valencies).[25] Figure 6b shows this for the octamolybdates together with the values for the oxygen atoms in $[Mo_8O_{26}F_2]^{6-}$. The different coordination types separate very well with the pseudoterminal (pt) nature of O10 discussed above. The bonding in $[Mo_8O_{26}F_2]^{6-}$ thus appears to be quite similar to that in octamolybdates with the $\{MoO_5F\}$ octahedra behaving like those in type II molybdates.

THERMAL STABILITY

The thermal stability of complex **3** was studied by temperature-dependent powder X-ray diffractometry (TD PXRD) and thermogravimetrical analysis (Figures S21 and S22, Supporting Information). In the temperature range up to 240 °C, only one pure phase of compound **3** was present in the powder diffraction patterns. Then, a sharp thermal transition takes place that can be associated with shift of peaks, especially with the most intensive ones at 2θ = 8.28°, 8.76° 9.18°, 10.00°, and 11.99°, which match the following Miller indices: $01\bar{1}$, $10\bar{1}$, $1\bar{1}0$, 110, and 002, respectively (Figure S20, Supporting Information). In the temperature range of 240−330 °C, another crystalline phase is visible before complete decomposition of the solid sample.

These processes are in a good agreement with DTA/TG analysis. For instance, the first thermal dehydration step proceeded in the temperature interval of 165−300 °C and is accompanied by the gradual release of 5 equiv of water molecules. Above this temperature, the mass spectroscopic detection reveals the irreversible decomposition with a gradual release of CO_2 (m/z = 44; associated with the ligand oxidation by difluorooctamolybdate), H_2O (m/z = 18), and organic components.

In the TGA experiment of compound **2** (Figure S19, Supporting Information), a dehydration step is observed within a temperature range of 60−240 °C; after that the collapse of the crystal structure occurs (Figure S18, Supporting Information).

MAGNETIC PROPERTIES

Both, the 2D (**2**) and the 3D (**3**) coordination networks are structurally based on linear trinuclear Co^{II} clusters acting as SBUs. Consequently, a magnetic study can give information about the expected magnetic coupling strength between the Co^{II} spin carriers. However, one has to bear in mind that one needs to deal with a combination of structurally very intricate networks and the complex electronic characteristics of high-spin Co^{II} spin centers. In the following, we will approach these issues with the aim to avoid a magnetochemical over-parametrization in the analyses of the magnetic susceptibility data, χ_m, starting with the study of compound **2** followed by compound **3**. The $\chi_m T(T)$ plot (Figure 7) of a polycrystalline

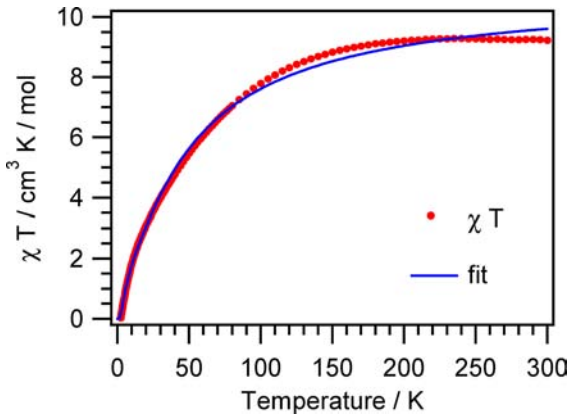

Figure 7. Thermal variation of $\chi_m T$ for **2** (solid line is a fit according to eq 1).

sample of **2** (scaled per Co_3 unit) exhibits decreasing $\chi_m T$ values on cooling, starting with 9.2 cm^3 K mol^{-1} at 300 K and approaching a zero value at 1.9 K. The high temperature $\chi_m T$ value is much higher than the spin-only value of 5.6 cm^3 K mol^{-1} for three noninteracting spins with S = 3/2 (g = 2.0) owing to the significant orbital contribution of Co^{II}; hence it expresses a sensible g value expected for Co^{II} ions. The low-temperature $\chi_m T$ values are significantly smaller than expected for three isolated octahedral Co^{II} magnetic centers. Thus, the shape of the curve is typical of polynuclear cobalt(II) compounds, and it clearly reflects contributions from antiferromagnetic exchange interactions along the chains combined with zero-field splitting of the cobalt(II) spin manifold. The corresponding $\chi_m(T)$ plot is given in Figure S23, Supporting Information.

The inverse magnetic susceptibility curve for **2** (Figure 8) shows a linear behavior in the temperature range from 190−

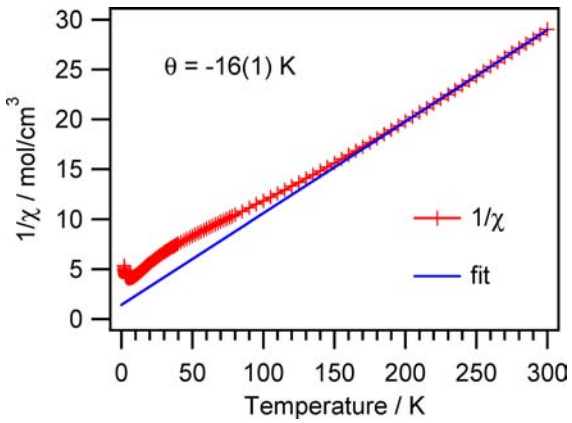

Figure 8. Inverse magnetic susceptibility vs temperature for **2** (solid line represents a Curie−Weiss fit in the temperature range 190−300 K).

300 K, and thus obeys the Curie−Weiss law with a Curie constant C = 3.6 cm^3 K mol^{-1} (per Co) and Θ = −16(1) K from which we can derive a g value of 2.8. Clearly, single-ion behavior of Co^{II} combined with magnetic exchange interactions

dx.doi.org/10.1021/ic400954x | Inorg. Chem. 2013, 52, 8784−8794

will contribute to the observed Θ value. The Curie constant C lies within the expected range for Co^{II}.[28]

In principle, an interpretation of magnetic susceptibility data from polynuclear, high-spin cobalt(II) species is complicated by the coexistence of large zero-field splittings, measured with the energy parameter, D, and magnetic exchange interactions described by an energy parameter, J. A comparison of different methods for fitting the corresponding susceptibility data for polynuclear cobalt(II) compounds has been presented by Halcrow et al.[29] In the actual case of compound **2**, the situation is even more complex: the cobalt centers of the crystallographically asymmetric unit exhibit different distortions from octahedral symmetry, either toward tetragonality for the central Co1 or additionally combined with a rhombic component for the two adjacent Co2 centers. Furthermore, the main ligand-field axes for neighboring coordination entities are distinctly tilt to each other. Next, one has to consider that different superexchange pathways are active for the magnetic coupling within the chains. They are related either to the triple bridge between Co1 and Co2 centers or to the quadruple bridge involving the μ-fluoro anions between adjacent Co2 metal ions. Consequently, the analysis of the resulting spin states reaches a high complexity. Therefore, the method of choice to model the magnetic data appears to be the empirical Rueff's approach,[30] which describes the deviation of the compound from Curie behavior using two different exponential terms, which contain contributions from zero-field splitting and magnetic exchange interactions. Here, this relationship is given in the version[31] of eq 1:

$$\chi_m = \left(\frac{N\beta^2 g^2}{3kT}\right)\left[(3.6-\alpha)\exp\left(-\frac{D}{kT}\right)+\alpha\exp\left(\frac{J}{kT}\right)\right] \quad (1)$$

where D is the zero-field splitting parameter, J is the magnetic exchange coupling parameter, and α is a dummy parameter to give a ratio between the component parts of the equation. A fit based on the experimental Curie constant of 3.6 cm^3 K mol^{-1} and a g value of 2.8 results in $|D/k| = 55(2)$ K and $J/k = -7.9(6)$ K ($\alpha = 1.27$). Comparison with other Co^{II} chain compounds shows that the values are in agreement with comparable literature values.[31] The fit looks acceptable in view of the complexity of the system. However, most importantly, one needs to bear in mind that the obtained J value gives only an estimate of the overall strength of the magnetic exchange interaction within the chains; in fact, the magnetic coupling scheme, which is based on the chemical structure of the chain, is of the type $-J'-J'-J''-J'-J'-$, where J' refers to the Co1–Co2 interactions and J'' to the Co2–Co2 interactions. To differentiate between these two parameters is certainly beyond the possibility of the applied method. Moreover, a detailed magnetostructural analysis of the coupling of $S = 3/2$ states can be of a very complex nature as well.[32]

Next, the $\chi_m T(T)$ plot (Figure 9) of a polycrystalline sample of **3** (scaled per Co_3 unit) exhibits decreasing $\chi_m T$ values on cooling, starting with 9.3 cm^3 K mol^{-1} at 300 K and approaching a zero value at 1.9 K. Overall, the shape of the curve is not too different from that of compound **2**. The corresponding $\chi_m(T)$ plot is given in Figure S24, Supporting Information.

The inverse magnetic susceptibility curve for **3** (Figure 10) shows a linear behavior in the temperature range from 150–300 K and thus obeys the Curie–Weiss law with a Curie constant $C = 3.6$ cm^3 K mol^{-1} (per Co) and $\Theta = -7.0(6)$ K.

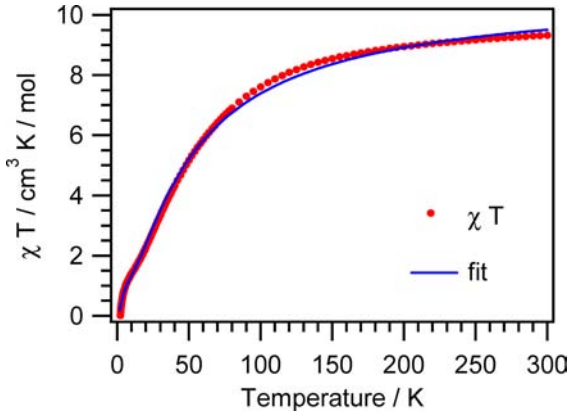

Figure 9. Thermal variation of $\chi_m T$ for **3** (solid line is a fit according to eq 1).

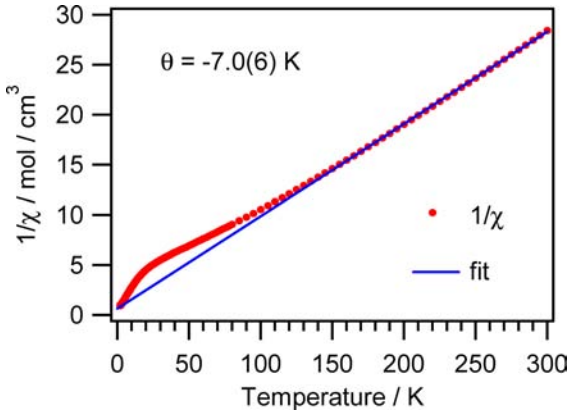

Figure 10. Inverse magnetic susceptibility vs temperature for **3** (solid line represents a Curie–Weiss fit in the temperature range 150–300 K).

In view of the similarity of the $\chi_m T(T)$ plots of compounds **2** and **3** and to quite a good extent also of their structural trinuclear Co^{II} units, it is tempting to apply the same method for the analysis of the magnetic susceptibility data. A quite acceptable fit based on the experimental Curie constant of 3.6 cm^3 K mol^{-1} and a g value of 2.8 results in $|D/k| = 48(2)$ K and $J/k = -4.3(9)$ K ($\alpha = 0.65$). The smaller J value for **3** is clearly reflected in the $\chi_m T(T)$ plot because of the sharp decrease in the $\chi_m T$ values at very low temperatures. However, as discussed above, the complexity of the chemical and structural system of **3** is still too high for allowing any detailed magnetostructural analysis.

CONCLUSION

We illustrated the interesting perspective of the flexible bistriazolyl ligand tr_2pr in the design of Co^{II}/Mo^{VI} fluorinated hybrid solids employing the hydrothermal method. The presence of aqueous HF in the reaction systems seems to be the most likely factor predetermining the Mo^{VI} oxofluoride condensation (**1**, **3**), while its absence, even at high excess of Co^{II}, resulted in the formation of the F^-/MoO_4^{2-} mixed-anion complex (**2**). The flexible bistriazole ligand (tr_2pr) displays a uniform tetradentate role adopting *anti–anti* or *anti–gauche*

dx.doi.org/10.1021/ic400954x | Inorg. Chem. 2013, 52, 8784–8794

conformations. A unique example of incorporation of difluorooctamolybdate anions $[Mo_8O_{26}F_2]^{6-}$ into the α-Po type coordination framework based on the $[Co_3(\mu_2\text{-tr})_6]^{6+}$ SBU has been given. The preformed open channels with a cross section of ~3 Å × 7 Å perfectly match the size of charge-compensating $[Mo_8O_{26}F_2]^{6-}$ anions. This anion exhibits an O-tetradentate binding mode toward $[Co_3(\mu_2\text{-tr})_6]^{6+}$ units, which results in their integration in a novel two-nodal 4,10-c net. The employment of a 1,2,4-triazole ligand family for the rational construction of MOFs with molybdenum oxide fluoride polyanions or mixed-anionic $F^-/Mo_xO_y^{n-}$ species can stimulate further studies of the complexes in the context of practical applications. Moreover, the study of magnetic properties of coordination network compounds is a very topical issue in the field of molecular magnetism.[33] In the present case, the magnetic susceptibility data for **2** and **3** reveal an average antiferromagnetic coupling strength (J/k) between the Co^{II} centers on the order of −8 and −4 K, respectively. The geometry of the $[Mo_8O_{26}F_2]^{6-}$ anion was optimized using density functional theory. The data demonstrate that the gas-phase VWN aproach is less suitable for study of oxyfluorides than it is for oxoanion analogues. The more ionic character of the Mo−F bond and the relatively high charge density of the $[Mo_8O_{26}F_2]^{6-}$ anion appear to require a higher level treatment.

■ ASSOCIATED CONTENT

Supporting Information

Crystallographic data, experimental details for X-ray structural analyses, and spectral characterization data. This material is available free of charge via the Internet at http://pubs.acs.org.

■ AUTHOR INFORMATION

Corresponding Author

*E-mail addresses: ab_lysenko@univ.kiev.ua (A.B. Lysenko); liu@iac.unibe.ch (S.-X. Liu).

Notes

The authors declare no competing financial interest.

■ ACKNOWLEDGMENTS

Financial support by Deutsche Forschungsgemeinschaft and by the Swiss National Science Foundation (Grant Nos. 200020-130266 and 200021-147143) is gratefully acknowledged.

■ REFERENCES

(1) (a) Michailovski, A.; Patzke, G. R. *Chem.—Eur. J.* **2006**, *12*, 9122. (b) Ye, Z. G.; Ravez, J.; Rivera, J. P.; Chaminade, J. P.; Schmid, H. *Ferroelectrics* **1991**, *124*, 281.

(2) (a) Heier, K. R.; Norquist, A. J.; Wilson, C. G.; Stern, C. L.; Poeppelmeier, K. R. *Inorg. Chem.* **1998**, *37*, 76. (b) Maggard, P. A.; Stern, C. L.; Poeppelmeier, K. R. *J. Am. Chem. Soc.* **2001**, *123*, 7742. (c) Mahenthirarajah, T.; Li, Y.; Lightfoot, P. *Dalton Trans.* **2009**, 3280. (d) Lin, H.; Yan, B.; Boyle, P. D.; Maggard, P. A. *J. Solid State Chem.* **2006**, *179*, 217. (e) Maggard, P. A.; Kopf, A. L.; Stern, C. L.; Poeppelmeier, K. R.; Ok, K. M.; Halasyamani, P. S. *Inorg. Chem.* **2002**, *41*, 4852. (f) Maggard, P. A.; Kopf, A. L.; Stern, C. L.; Poeppelmeier, K. R. *CrystEngComm* **2004**, *6*, 451.

(3) Kirsch, J. E.; Izumi, H. K.; Stern, L.; Poeppelmeier, K. R. *Inorg. Chem.* **2005**, *44*, 4586.

(4) Burkholder, E.; Zubieta, J. *Inorg. Chim. Acta* **2004**, *357*, 279.

(5) (a) Michailovski, A.; Rüegger, H.; Sheptyakov, D.; Patzke, G. R. *Inorg. Chem.* **2006**, *45*, 5641. (b) Michailovski, A.; Hussain, F.; Spingler, B.; Wagler, J.; Patzke, G. R. *Cryst. Growth Des.* **2009**, *9*, 2009.

(6) Kamenar, B.; Kaitner, B.; Strukan, N. *Acta Crystallogr.* **1990**, *C46*, 2249.

(7) Stover, A. K.; Gutnick, J. R.; Sarjeant, A. N.; Norquist, A. J. *Inorg. Chem.* **2007**, *46*, 4389.

(8) (a) Hagrman, P. J.; Hagrman, D.; Zubieta, J. *Angew. Chem., Int. Ed.* **1999**, *38*, 2638. (b) Pope, M. T.; Müller, A. *Polyoxometalate Chemistry From Topology via Self-Assembly to Applications*; Kluwer Academic: Dordrecht, the Netherlands, 2001.

(9) Aromí, G.; Barrios, L. A.; Roubeau, O.; Gamez, P. *Coord. Chem. Rev.* **2011**, *255*, 485.

(10) (a) Savard, D.; Cook, C.; Enright, G. D.; Korobkov, I.; Burchell, T. J.; Murugesu, M. *CrystEngComm* **2011**, *13*, 5190. (b) Ding, B.; Yang, E.-C.; Zhao, X.-J.; Wang, X. G. *J. Coord. Chem.* **2008**, *61*, 3793. (c) Ren, P.; Ding, B.; Shi, W.; Wang, Y.; Lu, T.; Cheng, P. *Inorg. Chim. Acta* **2006**, *359*, 3824. (d) Garcia, Y.; Guionneau, P.; Bravic, G.; Chasseau, D.; Howard, J. A. K.; Khan, O.; Ksenofontov, V.; Reiman, S.; Gutlich, P. *Eur. J. Inorg. Chem.* **2000**, 1531.

(11) (a) Lysenko, A. B.; Senchyk, G. A.; Lincke, J.; Lässig, D.; Fokin, A. A.; Butova, E. D.; Schreiner, P. R.; Krautscheid, H.; Domasevitch, K. V. *Dalton Trans.* **2010**, *39*, 4223. (b) Bondar, O. A.; Lukashuk, L. V.; Lysenko, A. B.; Krautscheid, H.; Rusanov, E. B.; Chernega, A. N.; Domasevitch, K. V. *CrystEngComm* **2008**, *10*, 1216.

(12) Sheldrick, G. M. *Acta Crystallogr.* **2008**, *A64*, 112.

(13) Rather, B.; Zaworotko, M. J. *Chem. Commun.* **2003**, 830.

(14) Senchyk, G. A.; Lysenko, A. B.; Krautscheid, H.; Domasevitch, K. V. *Inorg. Chem. Commun.* **2011**, *14*, 1365.

(15) (a) Berrocal, T.; Mesa, J. L.; Pizarro, J. L.; Bazán, B.; Iglesias, M.; Vilas, J. L.; Rojo, T.; Arriortua, M. I. *Dalton Trans.* **2010**, *39*, 834. (b) Kotsapa, E.; Weller, M. T. *Chem. Commun.* **2011**, *47*, 6132. (c) Berrocal, T.; Mesa, J. L.; Pizarro, J. L.; Lezama, L.; Bazan, B.; Arriortua, M. I.; Rojo, T. *J. Solid State Chem.* **2008**, *181*, 884.

(16) (a) Chakrabarti, S.; Natarajan, S. *Angew. Chem., Int. Ed.* **2002**, *41*, 1224. (b) Bazan, B.; Mesa, J. L.; Pizarro, J. L.; Goni, A.; Lezama, L.; Arriortua, M. I.; Rojo, T. *Inorg. Chem.* **2001**, *40*, 5691.

(17) Mandal, S.; Natarajan, S.; Greneche, J. M.; Riou-Cavellec, M.; Ferey, G. *Chem. Mater.* **2002**, *14*, 3751.

(18) Spek, A. L. *J. Appl. Crystallogr.* **2003**, *36*, 7.

(19) (a) Hagrman, P. J.; Zubieta, J. *Inorg. Chem.* **1999**, *38*, 4480. (b) Niu, Y.-Y.; Wang, L.-F.; Lv, X.-R.; Du, H.-J.; Qiao, Y.-Z.; Wang, H.-M.; Song, L.-S.; Wu, B.-L.; Hou, H.-W.; Ng, S. W. *CrystEngComm* **2011**, *13*, 5071.

(20) (a) Blatov, V. A. *IUCr CompComm Newsl.* **2006**, *7*, 4. (b) Blatov, V. A.; Shevchenko, A. P.; Serezhkin, V. N. *J. Appl. Crystallogr.* **2000**, *33*, 1193.

(21) (a) Courcot, B.; Bridgeman, A. J. *J. Comput. Chem.* **2011**, *32*, 1703. (b) Courcot, B.; Bridgeman, A. J. *J. Phys. Chem. A* **2009**, *113*, 10540.

(22) (a) te Velde, G.; Bickelhaupt, F. M.; van Gisbergen, S. J. A.; Fonseca Guerra, C.; Baerends, E. J.; Snijders, J. G.; Ziegler, T. *J. Comput. Chem.* **2001**, *22*, 931. (b) Fonseca Guerra, C.; Snijders, J. G.; te Velde, G.; Baerends, E. J. *Theor. Chem. Acc.* **1998**, *99*, 391. (c) ADF2012, SCM, Theoretical Chemistry, Vrije Universiteit, Amsterdam, The Netherlands, http://www.scm.com.

(23) (a) van Lenthe, E.; Baerends, E.; Snijders, J. *J. Chem. Phys.* **1993**, *99*, 4597. (b) van Lenthe, E.; Baerends, E.; Snijders, J. *J. Chem. Phys.* **1994**, *101*, 9783. (c) van Lenthe, E.; Ehlers, A.; Baerends, E. *J. Chem. Phys.* **1999**, *110*, 8943.

(24) (a) Klamt, A.; Schürmann, G. *J. Chem. Soc., Perkin Trans.* **1993**, *2*, 799. (b) Pye, C.; Ziegler, T. *Theor. Chem. Acc.* **1999**, *101*, 396.

(25) (a) Bridgeman, A. J.; Cavigliasso, G.; Ireland, L. R.; Rothery, J. *J. Chem. Soc., Dalton Trans.* **2001**, 2095. (b) Bridgeman, A. J.; Empson, C. J. *Chem.—Eur. J.* **2006**, *12*, 2252.

(26) Bridgeman, A. J. *J. Phys. Chem. A.* **2002**, *106*, 12151.

(27) (a) Welk, M. E.; Norquist, A. J.; Arnold, F. P.; Stern, C. L.; Poeppelmeier, K. R. *Inorg. Chem.* **2002**, *41*, 5119. (b) Maggard, P. A.; Nault, T. S.; Stern, C. L.; Poeppelmeier, K. R. *J. Solid State Chem.* **2003**, *175*, 27. (c) Withers, R. L.; Brink, F. J.; Liu, Y.; Norén, L. *Polyhedron* **2007**, *26*, 290.

(28) Carlin, R. L. *Magnetochemistry*; Springer-Verlag: Berlin, Heidelberg, 1986.

(29) Jones, L. F.; Kilner, C. A.; Halcrow, M. A. *New J. Chem.* **2007**, *31*, 1530.
(30) Rueff, J.-M.; Masciocchi, N.; Rabu, P.; Sironi, A.; Skoulios, A. *Chem.—Eur. J.* **2002**, *8*, 1813.
(31) (a) Keene, T. D.; Hursthouse, M. B; Price, D. J. *Cryst. Growth Des.* **2009**, *9*, 2604. (b) Keene, T. D.; Zimmermann, I.; Neels, A.; Sereda, O.; Hauser, J.; Bonin, M.; Hursthouse, M. B; Price, D. J.; Decurtins, S. *Dalton Trans.* **2010**, *39*, 4937. (c) Garcia-Couceiro, U.; Castillo, O.; Luque, A.; Garcia-Teran, J. P.; Beobide, G.; Roman, P. *Cryst. Growth Des.* **2006**, *6*, 1839. (d) Boča, R. *Coord. Chem. Rev.* **2004**, *248*, 757.
(32) (a) Decurtins, S.; Güdel, H. U.; Pfeuti, A. *Inorg. Chem.* **1982**, *21*, 1101. (b) Decurtins, S.; Güdel, H. U. *Inorg. Chem.* **1982**, *21*, 3598.
(33) (a) Kahn, O. *Molecular Magnetism*; VCH: Weinheim, Germany, 1993. (b) Pilkington, M.; Decurtins, S. *Chimia* **2000**, *54*, 593. (c) Thompson, L. K., Ed. *Magnetism: Molecular and Supramolecular Perspectives*; Coordination Chemistry Reviews; Elsevier: Amsterdam, **2005**; Vol. *249*, p 2549.